Theoretical and Applied Fracture Mechanics 1 (1984) 145–159
North-Holland

DAMAGE ACCUMULATION AND CRACK GROWTH IN BILINEAR MATERIALS WITH SOFTENING: APPLICATION OF STRAIN ENERGY DENSITY THEORY

A. CARPINTERI *

Istituto di Scienza delle Costruzioni, University of Bologna, Bologna, Italy

G.C. SIH

Institute of Fracture and Solid Mechanics, Lehigh University, Bethlehem, Pennsylvania 18015 U.S.A.

A pseudo-elastic damage-accumulation model is developed by application of the strain energy density theory. The three-point bending specimen is analyzed to illustrate the crack growth characteristics according to a linear elastic softening constitutive law that is typical of concrete materials. Damage accumulation is accounted for by the decrease of elastic modulus and fracture toughness. Both of these effects are assessed by means of the strain energy density functions in the elements around a slowly moving crack. The rate of change of the strain energy density factor S with crack growth as expressed by the relation $\mathrm{d}S/\mathrm{d}a = \text{constant}$ is shown to describe the failure behavior of concrete. Results are obtained for different loading steps that yield different slopes of lines in an S versus a (crack length) plot. The lines rotate about the common intersect in an anti-clockwise direction as the load steps are increased. The intersect shifts upward according to increase in the specimen size. In this way, the combined interaction of material properties, load steps and specimen geometry and size are easily analyzed in terms of the failure mode or behavior that can change from the very brittle to the ductile involving stable crack growth. An upper limit on specimen or structural size is established beyond which stable crack growth ceases to occur and failure corresponds to unstable crack propagation or catastrophic fracture. The parameters that control the failure mode are the threshold values of the strain energy density function $(\mathrm{d}W/\mathrm{d}V)_c$ and the strain energy density factor S_c.

1. Introduction

The response of material is known to depend on the combined effects of geometry, loading and defects that may or may not grow in the forms of cracks during loading. It is not always possible to sort out these individual effects [1,2] unless they are analyzed accordingly. Terminologies such as 'size and/or geometric' effects are often used to classify the variance of experimental results. One of the major difficulties is associated with the quantitative assessment of material damage during each loading step. The range of the constitutive equations that may be applied without considering material damage is not always clear. It is this loadhistory dependency of material damage associated with crack growth that this work will focus attention on.

The influence of specimen size on fracture toughness has been pointed out in [3]. The relative size of defects or cracks to the specimen can obviously alter the response of a system from brittle to ductile without changing the material. Nonhomogeneity that often occurs in material can lead to additional interaction effects [4]. Generally speaking, failure does not occur instantaneously. It initiates with subcritical crack growth prior to reaching the stage of unstable crack propagation. Within a limited scale range, say macroscopic, the aforementioned events can be referred to as local failure leading to global instability of the specimen or structural component. A complete description of this material damage process is necessary for predicting material behavior. The strain energy density criterion [5] is particularly suited for this purpose because it can consistently relate local and global failure modes. The initiation of macrocrack growth is associated with critical value $(\mathrm{d}W/\mathrm{d}V)_c$ of the strain energy density function while the incipient of unstable fracture with S_c being defined as $r_c\,(\mathrm{d}W/\mathrm{d}V)_c$. The area under the true stress and strain curve is $(\mathrm{d}W/\mathrm{d}V)_c$ and r_c is the critical ligament size of the material at global instability. Unless these phenomena are assessed

* Visiting Scientist at the Institute of Fracture and Solid Mechanics, Lehigh University, from August 1982 to March 1983.

quantitatively, no confidence can be placed in translating small specimen data to the design of large size structural components. Work on subcritical crack growth under monotonic or repeated loading has not progressed significantly in the past mainly because of the lack of a consistent theory for analyzing the problem.

An attempt will be made in this investigation to apply the strain energy density theory [5,6] for analyzing the material damage process of linear elastic-linear softening materials. A fundamental relationship of the form

$$\frac{dW}{dV} = \frac{S}{r}, \tag{1}$$

will be used with r being the distance measured from the crack tip. The analysis will be 'pseudo-elastic' in the sense that loading and unloading will follow a linear path although the global behavior can be nonlinear. Permanent damage of the material is accounted for in each step of loading through the critical value of the strain energy density function. The three-point bend specimen will be used. Since the energy stored per unit volume of material will change in accordance with specimen sizes, the crack growth characteristics will also be affected. The influence of material softening on global instability is also exhibited from the display of the finite element results. The so-called 'size effect' in fracture mechanics is clearly explained while the traditional concept of collapse load associated with global structure instability can also be regarded as a limiting case of the more general treatment based on strain energy density. The varying degree of material damage [1] can be obtained either by changing the load steps and/or specimen sizes of the same material. Numerical results will be obtained to verify what has been discussed above.

2. Material damage and crack growth model

Consider a three-point bending specimen as shown in Fig. 1 where the beam is displayed symmetrically about an edge crack of length a_0. A core region with radius r_0 is introduced such that the assumption of a continuum prevails without having to deal with the influence of material microstructure near the crack tip.

The material behavior is assumed to follow a linear elastic-linear softening stress-strain relationship as given in Fig. 2. The stress and strain are shown to increase proportionally up to the point of ultimate stress, u. After that, only the strain will increase while the stress decreases linearly to zero at point f. When the load is relaxed, say at p, then unloading can occur along the line 0p. The new bilinear constitutive relation then follows the path $0pf$. Irreversibility is thus invoked only due to the degradation of the elastic modulus [7,8]. The influence of plasticity is not included [2]. The slope of the line 0p obviously decreases as p approaches f.

2.1. Material resistance to damage

For an undamaged material element, the critical value $(dW/dV)_c$ corresponds to the area $0uf$ in

[1] By including the energy dissipated due to plastic deformation, there is no difficulty to treat failure modes varying from brittle fracture to plastic collapse or limit load on the basis of the strain energy density criterion.

[2] The method can easily be extended to include the effects of crack growth accompanied by plastic deformation [9].

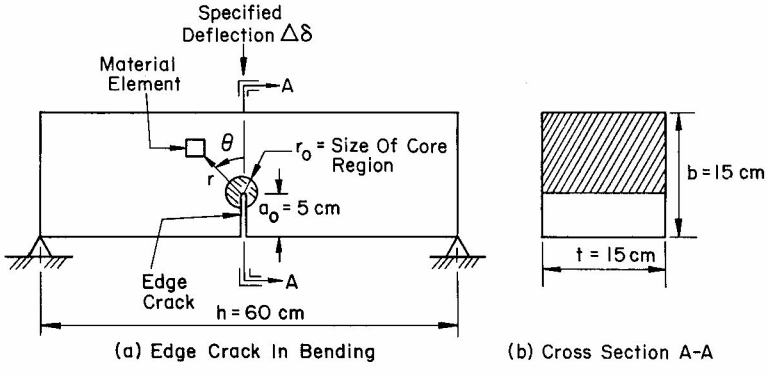

Fig. 1. Three-point bending specimen with an edge crack.

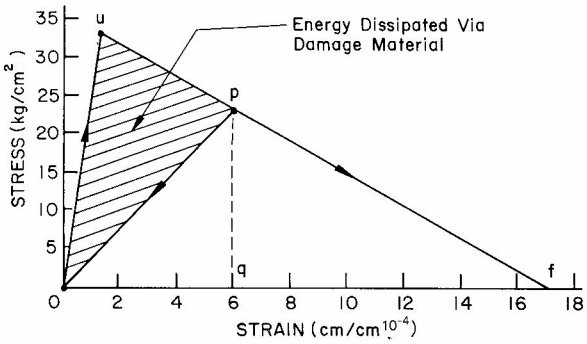

Fig. 2. Linear elastic-linear softening stress and strain relation.

Fig. 2. At p, the material element is assumed to be damaged with the area 0up denoted by $(\mathrm{d}W/\mathrm{d}V)_{\mathrm{d}}$ as the dissipated strain energy density function. Hence, the available energy density becomes

$$\left(\frac{\mathrm{d}W}{\mathrm{d}V}\right)_{\mathrm{c}}^{*} = \left(\frac{\mathrm{d}W}{\mathrm{d}V}\right)_{\mathrm{c}} - \left(\frac{\mathrm{d}W}{\mathrm{d}V}\right)_{\mathrm{d}} = \left(\frac{\mathrm{d}W}{\mathrm{d}V}\right)_{\mathrm{r}} + \left(\frac{\mathrm{d}W}{\mathrm{d}V}\right)_{\mathrm{a}}, \tag{2}$$

in which $(\mathrm{d}W/\mathrm{d}V)_{\mathrm{r}}$ is the amount that is recoverable corresponding to $0pq$ and $(\mathrm{d}W/\mathrm{d}V)_{\mathrm{a}}$ is the additional amount qpf. The slope 0p shall be denoted by E^*. Let σ_u and ε_u be the stress and strain correspond to the point u and ε_f to f with $\sigma_f = 0$. Then the relation between σ and ε for a typical point p can be written as

$$\sigma = \varepsilon E^* = \frac{\sigma_u \varepsilon_f}{(\varepsilon_f - \varepsilon_u) + (\sigma_u / E^*)}. \tag{3}$$

It follows that the various quantities $(\mathrm{d}W/\mathrm{d}V)$, $(\mathrm{d}W/\mathrm{d}V)_{\mathrm{d}}$, etc., can be expressed in terms of σ, ε, σ_u and ε_u as follows:

$$\left(\frac{\mathrm{d}W}{\mathrm{d}V}\right) = \tfrac{1}{2}(\sigma\varepsilon + \sigma_u\varepsilon - \sigma\varepsilon_u); \quad \left(\frac{\mathrm{d}W}{\mathrm{d}V}\right)_{\mathrm{r}} = \tfrac{1}{2}\sigma\varepsilon,$$

$$\left(\frac{\mathrm{d}W}{\mathrm{d}V}\right)_{\mathrm{d}} = \tfrac{1}{2}(\sigma_u\varepsilon - \sigma\varepsilon_u);$$

$$\left(\frac{\mathrm{d}W}{\mathrm{d}V}\right)_{\mathrm{c}}^{*} = \tfrac{1}{2}(\sigma_u\varepsilon_f - \sigma_u\varepsilon + \sigma\varepsilon_u). \tag{4}$$

As p moves between u and f, the effective modulus E^* alters accordingly and can be discretized into 25 different values and expressed in terms of E as

$$E^*(n) = \frac{(26-n)}{25}E, \quad n = 1, 2, \ldots, 25. \tag{5}$$

Table 1
Properties of three different materials

Material type	Final strain ε_f ($\times 10^{-4}$ cm/cm)	Critical strain energy density $(\mathrm{d}W/\mathrm{d}V)_{\mathrm{c}}$ ($\times 10^{-3}$ kg/cm^2)
A	16.87	26.90
B	8.87	14.14
C	4.87	7.77

Three different types of constitutive relations will be used. They correspond to concrete-like materials with the following general properties:

$$E = 365{,}000 \text{ kg/cm}^2; \qquad \nu = 0.1;$$
$$\sigma_u = 31.90 \text{ kg/cm}^2. \tag{6}$$

Only the final strains ε_f will change as shown in Table 1 and they are distinguished as Material A, B and C. Figures 3 and 4 display the results of E^* and $(\mathrm{d}W/\mathrm{d}V)_{\mathrm{c}}^*$ varying with $\mathrm{d}W/\mathrm{d}V$. The resistance of material to fracture thus far varies according to the energy state $\mathrm{d}W/\mathrm{d}V$ that is obtained from a finite element stress analysis. Up to the energy level

$$\frac{\mathrm{d}W}{\mathrm{d}V} = \tfrac{1}{2}\sigma_u\varepsilon_u = 1.39 \times 10^{-3} \text{ kg/cm}^2, \tag{7}$$

no damage will occur.

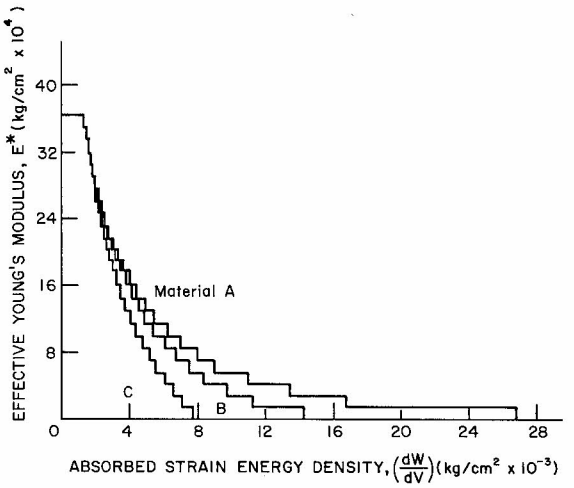

Fig. 3. Effective modulus as a function of absorbed strain energy density.

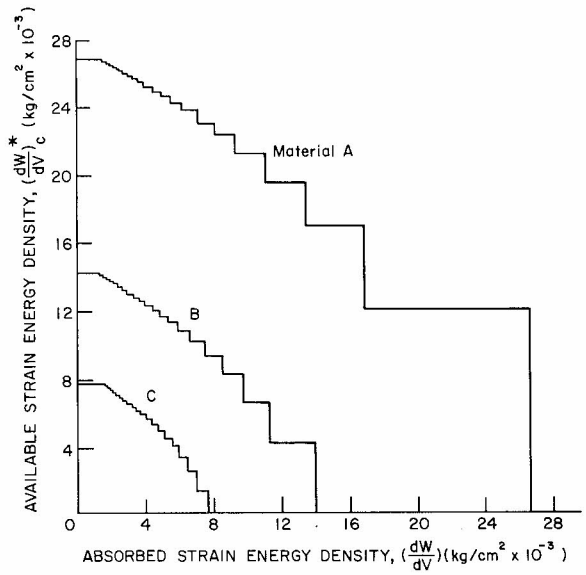

Fig. 4. Available strain energy density versus absorbed strain energy density function.

2.2. Strain energy density theory

The crack growth increment for each load step will be analyzed by the strain energy density theory of Sih [5,6]. This theory is based on the following assumptions.

(1) A core regions of radius r_0 is introduced around the crack tip which defines the limit of the continuum mechanics analysis.

(2) The strain energy density function dW/dV can, in general, be expressed in terms of S and r as in equation (1) where S can depend on two or three space variables.

(3) In consistent with Beltrami's criterion, the failure of material elements ahead of the crack corresponds to some critical value $(dW/dV)_c$. This leads to an increment of crack growth Δa:

$$\Delta a = r = \frac{S}{(dW/dV)_c}, \tag{8}$$

where S is the current value obtained from a stress analysis and Δa corresponds to the direction of S_{min} obtained by minimizing S with reference to the appropriate space variables.

The subcritical crack growth is assumed to follow the relation

$$\left(\frac{dW}{dV}\right)_c = \frac{S_1}{r_1} = \frac{S_2}{r_2} = \ldots = \frac{S_j}{r_j} = \text{const.} \tag{9}$$

This process may lead to either crack arrest or unstable crack growth depending on whether S_j and r_j in equation (8) approach (S_0, r_0) or (S_c, r_c).

The critical value S_c is characteristic of the material and can be related to the commonly known fracture toughness value K_{1C} [6] by the relation

$$S_c = \frac{(1+\nu)(1-2\nu)}{2\pi E} K_{1C}^2. \tag{10}$$

Values of S_c for a class of engineering materials can be found in [6].

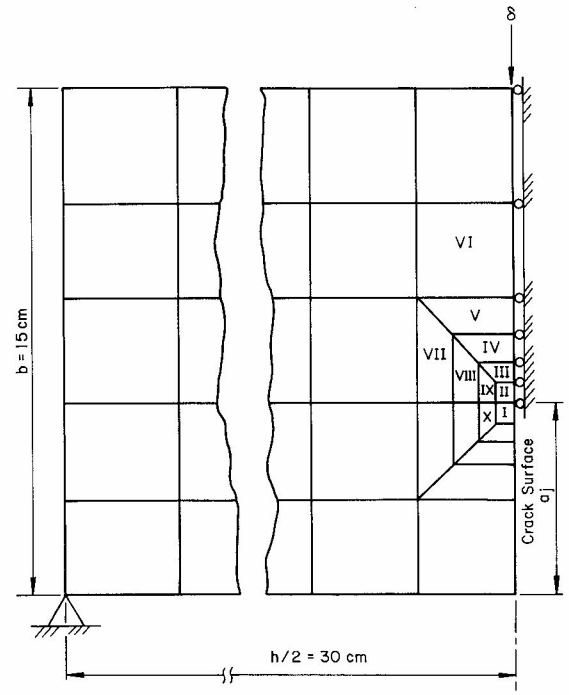

Fig. 5. Finite element grid pattern for one-half of the beam specimen and locations of damaged elements.

3. Three-point bend specimens: stresses and failure analysis

Referring to Fig. 1, the specimen assumes a width $b = 15$ cm, length $l = 60$ cm, thickness $t = 15$ cm and a crack length of $a_0 = 5$ cm. These dimensions will be scaled proportionally in the work to follow when studying the effect of specimen sizes on the load carrying capacity of the system.

Because of symmetry about the load line of action, only one-half of the geometry represented

in Fig. 1 needs to be analyzed. The finite element grid pattern is displayed in Fig. 5 such that the stress and energy state for each increment of load will be calculated by application of the Axisymmetric/Planar Elastic Structures (APES) computer program [10]. A total of 309 nodes and 52 elements are employed to generate the mesh in Fig. 5. Use is made of the twelve (12) nodes quadrilateral isoparametric elements allowing for cubic displacements and quadratic stress and strain fields in each element. The r^{-1} singular strain energy density field is embedded into the crack tip region by means of the 1/9 to 4/9 nodal spacing on elements adjacent to the crack.

3.1. Material damage and crack growth analysis

The specimen is displaced incrementally and five different cases will be analyzed as described in Table 2. For Case No. (1), six displacement steps were chosen with the corresponding values of load P versus deflection δ and crack growth increment Δa for each step given in Table 3. In general, the elements nearest to the crack front are more severely damaged than those further away. The degree of damage is measured by the change in the local effective moduli E^* such that damage increases on a scale of 1 to 25 in accordance with equation (5). The undamaged elements are not numbered and the material is assumed to behave elastically in compression. With reference to Fig. 5, the damage levels within the ten elements nearest to the crack tip region labelled as I, I,,..., X are computed for each increment of crack growth. The results for the five different cases in Table 3 are tabulated in Table 4. More specifically, it can be seen from Table 3 or 4, that the crack length $a_j (j = 1, 2,$ etc.) increases for each increment of loading and the growth increment Δa is nonuniform. With reference to Case No. (1), the material

Table 2
Incremental displacement applied to bend specimen

Case No.	Material type	Displacement increment $\Delta\delta$ ($\times 10^{-3}$ cm)
(1)	A	4.0
(2)	B	4.0
(3)	C	4.0
(4)	C	2.0
(5)	C	1.0

Table 3
Load and displacement increments for different cases

Increment $j = 1, 2,$ etc.	Load P_j (kg)	Deflection δ_j ($\times 10^{-3}$ cm)	Crack growth increment Δa (cm)
Case No. (1)			
1	574	4	0.088
2	967	8	0.089
3	996	12	0.476
4	706	16	1.346
5	400	20	1.667
6	238	24	1.603
Case No. (2)			
1	564	4	0.157
2	828	8	0.480
3	572	12	1.688
4	276	16	2.000
Case No. (3)			
1	528	4	0.420
2	582	8	1.408
3	287	12	2.190
Case No. (4)			
1	302	2	0.069
2	521	4	0.421
3	566	6	0.809
4	384	8	1.533
5	166	10	2.000
Case No. (5)			
1	152	1	0.023
2	301	2	0.069
3	426	3	0.166
4	483	4	0.444
5	500	5	0.506
6	392	6	1.110
7	273	7	1.208
8	119	8	1.629

elements I, II, III and IX being closest to the crack tip are damaged for the first increment of $\Delta\delta_1 = 4 \times 10^{-3}$ cm. The crack advances from 5.088 cm to 5.177 cm. More elements are damaged resulting in larger crack growth increments. By the 5th and 6th load increment, $\delta_5 = 20 \times 10^{-3}$ cm and $\delta_6 = 24 \times 10^{-3}$ cm, all the ten elements around the crack front are permanently damaged. Elements I, II, III, IV and IX have all reached the maximum damage level 25. Element VI always attains the lowest number as it is furthest away from the crack. Similar trends are observed for the remaining cases. Case No. (3) corresponding to Material C with the lowest ε_f value cannot sustain as much damage in crack growth as Materials A and B. The final crack length a_3 is smaller than a_6 and a_4 in Cases No. (1) and (2), respectively. The data in Cases No. (4) and (5) correspond to the

Table 4
Damage accumulation data for the five cases in Table 3

Deflection δ_j ($\times 10^{-3}$ cm)	Crack length a_j (cm)	Damage element reference number I	II	III	IV	V	VI	VII	VIII	IX	X
Case No. (1)											
4	5.088	7	18	4	–	–	–	–	–	4	–
8	5.177	21	24	22	11	–	–	–	10	18	9
12	5.653	25	25	25	23	15	–	9	19	23	12
16	6.999	25	25	25	25	23	9	13	21	25	12
20	8.666	25	25	25	25	24	14	13	21	25	18
24	10.269	25	25	25	25	24	1	13	21	25	21
Case No. (2)											
4	5.157	7	19	4	–	–	–	–	–	5	–
8	5.637	23	25	24	12	–	–	–	11	20	9
12	7.325	25	25	25	24	17	–	9	20	23	9
16	9.325	25	25	25	25	22	6	9	21	25	9
Case No. (3)											
4	5.420	8	22	4	–	–	–	–	–	5	–
8	6.828	25	25	25	14	–	–	–	12	23	7
12	9.000	25	25	25	25	17	–	6	21	25	7
Case No. (4)											
2	5.069	–	2	–	–	–	–	–	–	–	–
4	5.490	8	22	4	–	–	–	–	–	5	–
6	6.299	21	25	23	6	–	–	–	3	16	–
8	7.832	25	25	25	22	2	–	–	9	17	–
10	9.832	25	25	25	25	12	–	–	9	17	–
Case No. (5)											
1	5.023	–	–	–	–	–	–	–	–	–	–
2	5.092	–	2	–	–	–	–	–	–	–	–
3	5.258	–	15	–	–	–	–	–	–	–	–
4	5.702	8	25	8	–	–	–	–	–	2	–
5	6.208	18	25	22	2	–	–	–	–	8	–
6	7.318	25	25	25	13	–	–	–	–	8	–
7	8.526	25	25	25	20	–	–	–	–	8	–
8	10.155	25	25	25	25	–	–	–	–	8	–

same Material C but with lower deflection increments. This enhances slow crack growth, a result that is frequently observed in experiments.

3.2. Load-displacement relationships

Applying the crack growth-damage model discussed earlier, the load P also increases in a stepwise fashion according to the specified deflection δ. It is therefore instructive to trace the softening behavior by observing the load P versus deflection δ relationship. A typical schematic representation of this relationship is shown in Fig. 6 which consists of six steps. The point C is obtained by a linear extrapolation of the previous point (P, δ) and the origin assuming a constant secant modulus. A decrease in secant modulus is then determined by the damage analysis to point D in accordance with the strain energy density theory and the values of E^* and $(\mathrm{d}W/\mathrm{d}V)_c^*$ are adjusted according to Figs. 3 and 4. A crack growth analysis is then performed to locate the point E. The specimen then acquires a new tangent modulus. Softening starts with additional loading. Now, the tangent modulus becomes negative with decreasing load. A damage analysis is made and followed by a crack growth analysis using the APES computer program. The ratio CD/CE represents the amount of stiffness loss due to material damage while DE/CE corresponds to that due to crack growth. According to Fig. 6, $CD \simeq DE$ at the fourth load increment. The influence of crack growth begins to dominate during the fifth and sixth step of loading. By then, the specimen supports only one-fifth of the maximum load and the crack has penetrated two-thirds of the specimen width. The ratio CD/CE or DE/CE is sensitive to the way the specimen is loaded incrementally. Material damage and

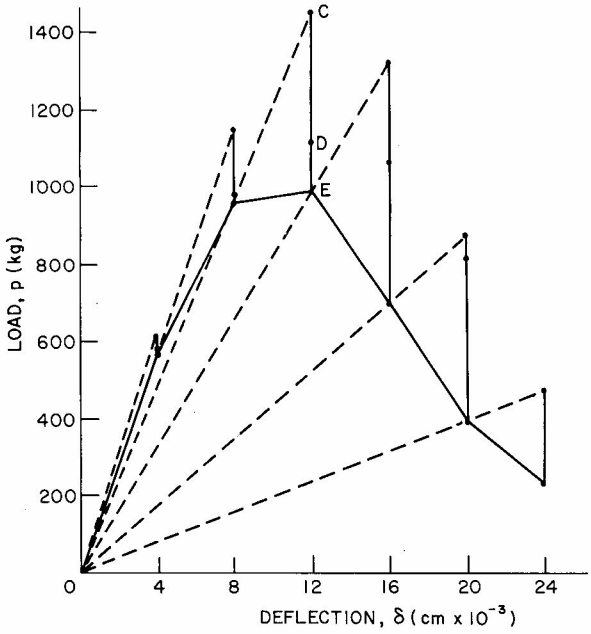

Fig. 6. Typical schematic relation of load versus deflection of three-point bend specimen.

crack growth are by nature load-history dependent. This point will be discussed in more detail subsequently.

3.3. Strain energy density function

It is informative to plot the strain energy density contours around the crack tip region from which failure initiates or occurs. Typical contours for Case No. (4) corresponding to the first and fifth loading step are shown in Figs. 7 and 8, respectively. Results are displayed only for a portion of the crack tip region, 0.5 cm in length. The magnitude of dW/dV in units of kg/cm^2 increases with decreasing r becoming unbounded as r approaches zero. A quantitative assessment of this decay can be seen from the magnitudes of the various dW/dV = const. contours in Figs. 7 and 8 with the dark region being nearest to the crack tip. The gradient of dW/dV as a function of r becomes more pronounced as the loading step is increased. The variation of dW/dV in the angular direction can be related to material failure by yielding and/or crack growth. This will be discussed subsequently.

3.4. Comparison of material damage with yielding

It is of interest to compare the locations of damage zone obtained from the quasi-linear analysis with yielding predicted from the strain energy density criterion [5,6]. Let damage in the jth element be measured by the reduction in the elastic modulus as

$$d_j = \frac{E - E_j^*}{E}. \tag{11}$$

With reference to the centroids (x_j, y_j) of the element, the center of the damage zone may be determined by

$$x_d = \sum_j \frac{x_j d_j A_j}{\sum_j d_j A_j}, \qquad y_d = \sum_j \frac{y_j d_j A_j}{\sum_j d_j A_j}, \tag{12}$$

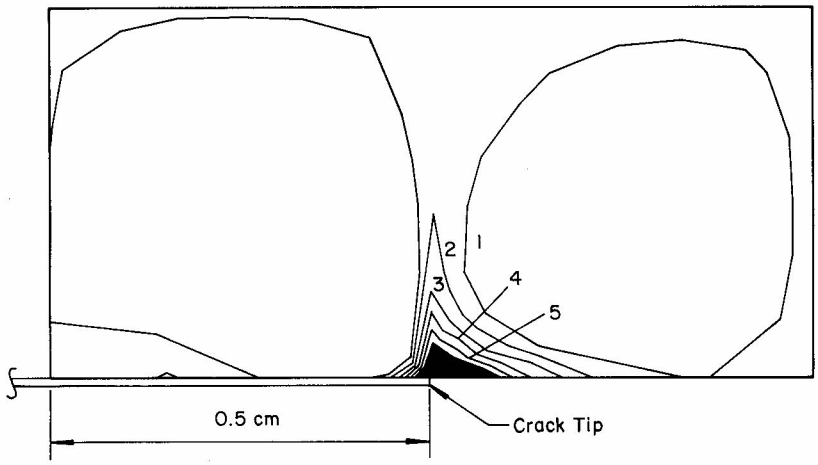

Contour No. 1 - 0.04 x 10^{-3} kg/cm^2
2 - 1.60 x 10^{-3}
3 - 3.30 x 10^{-3}
4 - 4.90 x 10^{-3}
5 - 6.50 x 10^{-3}
Dark Region ≥ 8.10 x 10^{-3}

Fig. 7. Strain energy density contours around the crack tip for the first loading step of Material C, Case No. (4).

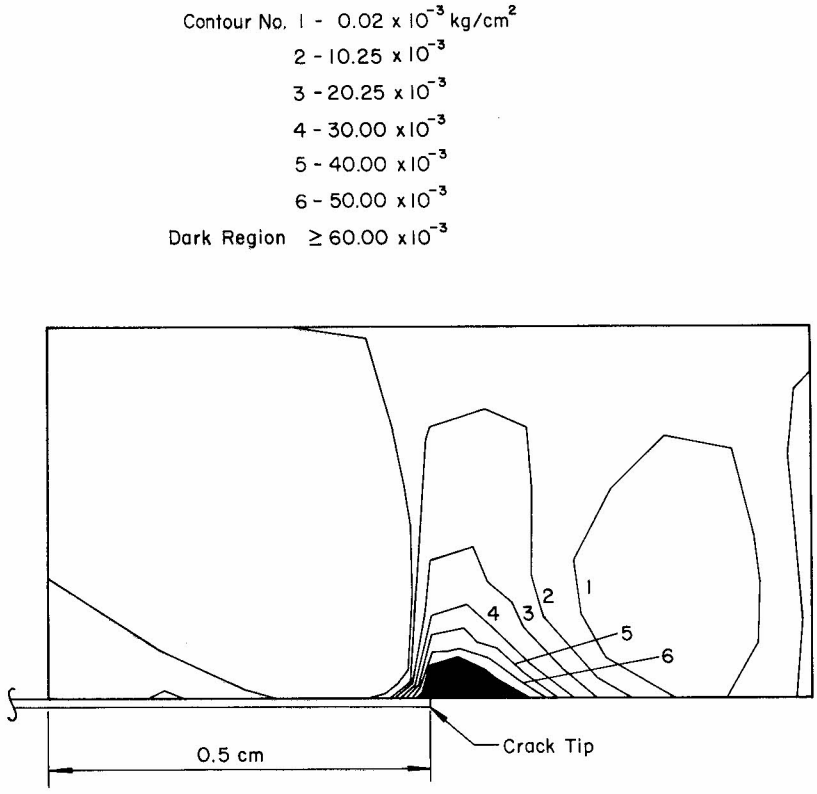

Fig. 8. Strain energy density contours around the crack tip for the fifth loading step of Material C, Case No. (4).

where A_j is the area of an element. These locations for Cases No. (3), (4) and (5) are plotted in Fig. 9 with reference to the crack tip position. They tend to congregate off to the side of the crack and bend towards the specimen boundary perpendicularly as the distance r is increased.

By using the asymptotic elastic stress solution, the strain energy density factor S can be calculated as a function of θ measured from the line of expected crack growth which corresponds to the vertical line or crack plane in Fig. 9. The relative minimum S can be shown to correspond with $\theta_0 = 0°$ and relative maximum with $\theta_p = \cos^{-1}(1 - 2\nu)$. According to the S-criterion [5,6], the former refers to the direction of macrocrack growth and the latter to the direction of maximum yielding. For $\nu = 0.1$, an angle of $\theta_p = 36.8°$ is predicted. The agreement is quite good for small values of r. This is to be expected as the asymptotic stress solution is limited to $r/a < 1/10$. Yielding can thus be viewed as damage with loss of material stiffness.

4. Discussion of results: material, loading increment and size effects

Material response is, to say the least, a complex behavior as it depends on many variables. The results obtained on the three-point bend specimen are useful to understand how the individual variables will affect the behavior of concrete-like materials that undergo softening on the stress-strain curve.

4.1. Difference in material

The three materials analyzed differ in their final strain ε_f as specified in Table 1. For a constant deflection increment of, say $\Delta\delta = 4 \times 10^{-3}$ cm, the P versus δ behavior is shown in Fig. 10. The shapes of the curves are similar but the areas under the curves are substantially different. Material A having the largest ε_f can sustain more load steps and absorb more energy.

The load P may also be plotted against crack

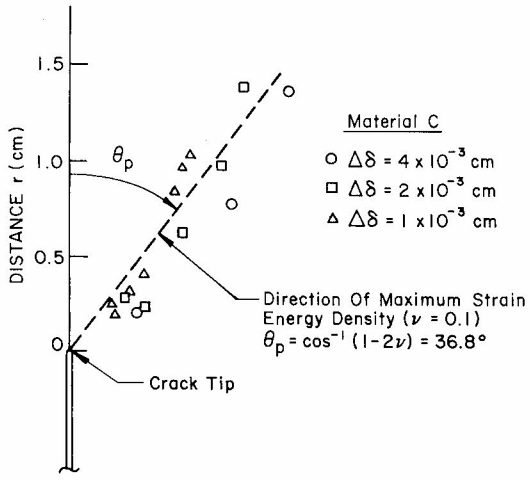

Fig. 9. Comparison of locations of damage centers with those of yielding.

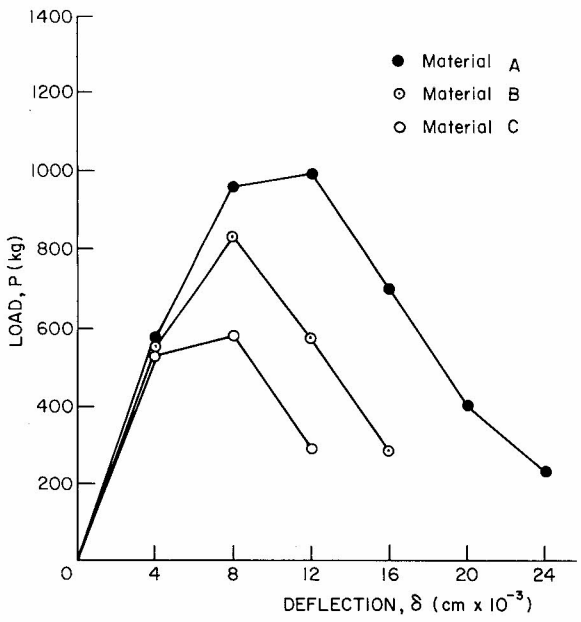

Fig. 10. Load-deflection for three different materials with $\Delta\delta = 4\times10^{-3}$ cm.

growth with P increasing with crack length and decaying after it reaches a peak. The trends for the three materials are similar to the P versus δ variations in Fig. 10 and will not be shown. The P-a curves are associated with the commonly known 'R-curves' in fracture mechanics. The peaks of these curves are usually considered as the transition between stable and unstable crack growth. This is, of course, not always correct because load transition involves the loss of structure stiffness due to both of material damage and crack growth. As it is distinguished in this work, unstable crack growth is governed by S_c while local material damage depends on $(dW/dV)_c^*$. The proportion of contribution by material damage and crack growth will vary depending on the combination of loading step, specimen size and material. For instance, for the smaller specimen with high fracture toughness, the traditional structural collapse mode of failure may precede unstable crack propagation. Only for the very large specimen where sufficient energy is stored and released suddenly, crack instability mode would dominate rather than the traditional structural collapse. It is therefore important to be able to assess failure modes corresponding to varying degrees of local material damage and crack growth as their combination controls the behavior of structures.

For the reasons just mentioned, it would be more correct to consider the relations between the strain energy density S and the crack length a. The results for Materials A, B and C are given in Fig. 11. Even though the physical process of material damage is a nonlinear function of P and δ, the data when interpreted in the S versus a diagram become linear [3], i.e., the condition $dS/da = \text{const.}$ is seen to prevail. These straight line relations correspond to the situations when both crack growth and the structure behavior are stable and obviously do not hold in general when the structure is near its post-collapse condition. The curve corresponding to Material A with the larger $(dW/dV)_c$ or fracture toughness has the larger slope. This implies that for a constant S_c, Material A can sustain a smaller critical crack length. This result is consistent with experimental observation on materials with varying degree of ε_f. In general, the slope of the S versus a curve is directly proportional to ε_f. A slow crack growth threshold strain energy density factor S_0 also appears to occur at the point where all the curves in Fig. 11 intersect. Note that dS/da possesses the same units as $(dW/dV)_c$ and the ratio $dS/da/(dW/dV)_c$ is

[3] The so-called 'R-curves' in fracture mechanics are nonlinear and must be obtained experimentally as the physical parameters are altered. They serve little purpose in design as they cannot be used to gather information for cases other than those already tested.

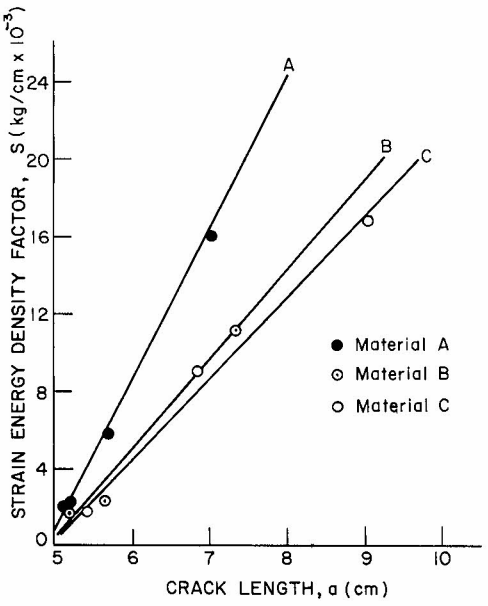

Fig. 11. Strain energy density factor versus crack length for three different materials with $\Delta\delta = 4\times10^{-3}$ cm.

always less than unity. This ratio can serve as a relative measure of material damage to crack growth. In the limit as $dS/da/(dW/dV)_c$ tends to unity, the structure will fail strictly by brittle fracture with no prior damage of material as in the classical linear elastic fracture mechanics theory.

4.2 Effect of loading steps

The effect of loading steps is analyzed for Material C with $\Delta\delta = 4\times10^{-3}$, 2×10^{-3} and 1×10^{-3} cm. Displayed in Fig. 12 are the curves for load P versus deflection δ. Within the range considered, the load carrying capacity of the specimen tends to increase with increasing load step. An increase of 36% in P_{max} corresponds to $\Delta\delta$ changing from 1×10^{-3} to 8×10^{-3} cm. This seems to reflect the usual increase in flexural strength of cement and mortar [11] when the applied strain rate is increased. Further increase in $\Delta\delta$ to 16×10^{-3} cm leads to a drop in P_{max} that is not shown here.

The effect of loading steps can be more clearly exhibited by plotting the strain energy density factor S as a function of crack length a for Material C as it is done in Fig. 13. The three lines with different slopes of dS/da correspond to $\Delta\delta = 4\times10^{-3}$, 2×10^{-3} and 1×10^{-3} cm. The slope dS/da increases as $\Delta\delta$ is increased. This means that for a given material with S_c = const., the critical crack length decreases if large loading steps are taken. This result is important for assessing the loading capacity of cement composites in terms of the interaction of loading steps with critical flaw size. The trend of the curves in Fig. 13 corresponds to that observed experimentally.

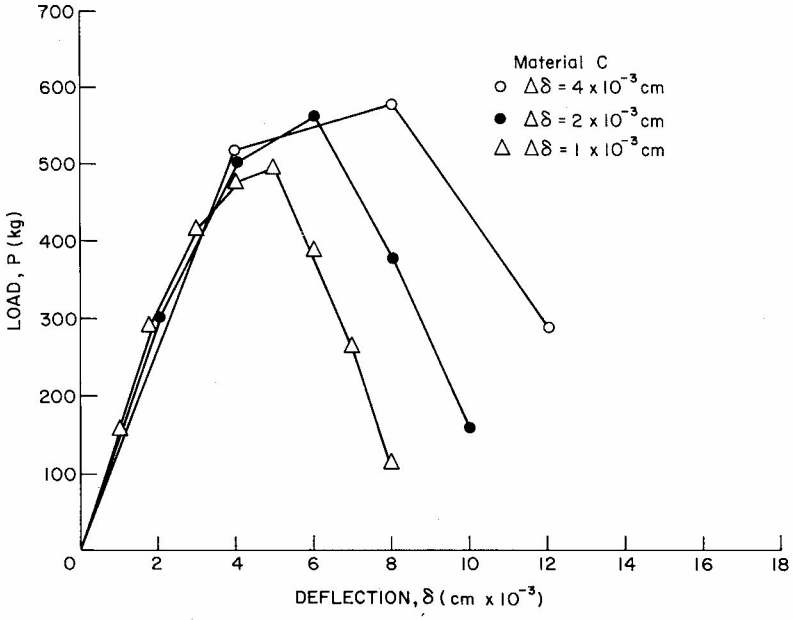

Fig. 12. Load-deflection for Material C with three different loading steps.

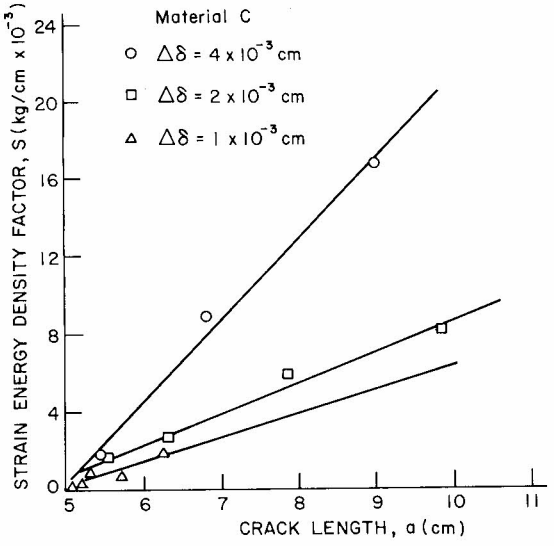

Fig. 13. Strain energy density factor versus crack length for Material C and three different loading steps.

4.3 Scaling in size

Because material damage and crack growth occur in a non self-similar fashion for each step of loading, different sizes of specimen appears to behave differently. This well-known size effect will be analyzed by the results obtained on the three-point bend specimen.

Let the load step to specimen width ratio be $\Delta\delta/b = 2.6 \times 10^{-4}$ for Material C while three different scales of specimen sizes are considered such that the dimension b in Fig. 1 differs by factors of 1, 2 and 3. Referring to Fig. 14 for a plot of P versus δ, the end points of the curve along the δ-axis also follow the scaling factors of 1, 2 and 3 while the factors 1, 4 and 9 are observed on the P-axis. The above scaling can be justified by means of dimensional analysis. A dimensionless load parameter may be defined

$$\frac{P}{(\mathrm{d}W/\mathrm{d}V)_c b^2} = \pi\left[\frac{\delta}{b}, \frac{E}{(\mathrm{d}W/\mathrm{d}V)_c}, \frac{\sigma_u}{(\mathrm{d}W/\mathrm{d}V)_c}, \nu, \frac{l}{b}, \frac{t}{b}, \frac{a_0}{b}\right], \tag{13}$$

as in the Buckingham's theorem for physical similitude in scale modelling. In equation (13), the material toughness $(\mathrm{d}W/\mathrm{d}V)_c$ and specimen width b have been used as the fundamental quantities. The dimensionless load parameter may be regarded as a function of the dimensionless deflection parameter δ/b only if all others are kept constant. In particular, since S depends on a, dimensional analysis can again yield a relation involving

$$\frac{S}{(\mathrm{d}W/\mathrm{d}V)_c b} = \Phi\left[\frac{a}{b}, \frac{E}{(\mathrm{d}W/\mathrm{d}V)_c}, \frac{\sigma_u}{(\mathrm{d}W/\mathrm{d}V)_c}, \nu, \frac{l}{b}, \frac{t}{b}, \frac{a_0}{b}\right]. \tag{14}$$

Knowing the values of S_0 for different b, the function Φ can be regarded as linear in a/b:

$$\frac{S}{(\mathrm{d}W/\mathrm{d}V)_c b} = \frac{\mathrm{d}S/\mathrm{d}a}{(\mathrm{d}W/\mathrm{d}V)_c}\frac{a-a_0}{b} + \frac{S_0}{(\mathrm{d}W/\mathrm{d}V)_c b}, \tag{15}$$

which may obviously be rearranged into the form

$$\frac{S}{(\mathrm{d}W/\mathrm{d}V)_c b} = A^*\left(\frac{a}{b}\right) + B^*. \tag{16}$$

The constants A^* and B^* are dimensionless and scale independent. Figure 15 gives the straight line plots for S versus $a - a_0$ with b varying from 15 cm to 222 cm. For a fixed $\Delta\delta/b$ ratio of 2.6×10^{-4} and material, all the lines are parallel. For Material C with the critical value $S_c = 8 \times 10^{-3}$ kg/cm, the limiting size is $b = 222$ cm. It shows that the critical crack growth size decreases with increasing specimen size, a conclusion that is well-known in practice.

Summarized in Fig. 16 are the relations between $P/(\mathrm{d}W/\mathrm{d}V)_c b^2$ and δ/b for $b = 15, 30, \ldots, 222$ cm. The vertical lines with the arrows indicate the limiting values of δ/b as the critical strain energy density value of $S_c = 8 \times 10^{-3}$ kg/cm is reached. This corresponds to $K_{1C} = 143.36$ kg/cm$^{3/2}$ which is typical for concrete [12]. It is clear that crack instability occurs for smaller deflection of the specimen as the size b is increased. Without considering unstable crack propagation, the maximum load can be estimated from the relation

$$P_{\max} = 332.90\left(\frac{\mathrm{d}W}{\mathrm{d}V}\right)_c b^2. \tag{17}$$

Figure 16 shows that structural instability or collapse occur before unstable crack propagation only in the case of $b = 15$ cm. For $b = 30$ cm, softening behavior is not present and the crack started to

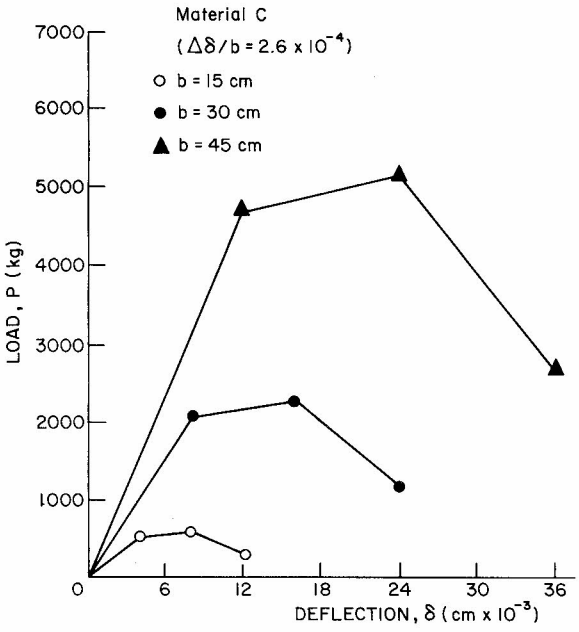

Fig. 14. Load-deflection for three different size and geometrically similar specimens with $\Delta\delta/b = 2.6\times10^{-4}$.

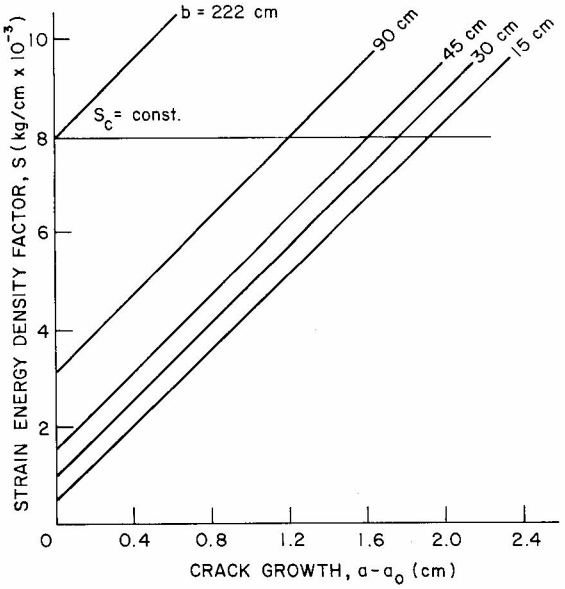

Fig. 15. Strain energy density factor versus crack length for Material C with $\Delta\delta/b = 2.6\times10^{-4}$.

spread in an unstable manner when the load P is still in the ascending stage. The critical crack length a_{cr} for each case can be found from the S versus a plots on Fig. 15. A similar set of curves are produced for Material C with $\Delta\delta/b = 0.65 \times 10^{-4}$ and they are given in Figs. 17 and 18. They basically show that with the same critical value S_c, the limiting specimen size is increased from $b = 222$ cm to 375 cm as the ratio $\Delta\delta/b$ is changed from 2.6×10^{-4} to 0.65×10^{-4}. The interaction of loading step with specimen size is also exhibited.

It is now apparent that the quantity $S_c/(dW/dV)_c b$ can also enter into the dimensional analysis in equation (13). In fact, for estimating P_{max}, it suffices to consider [4]

$$\frac{P_{max}}{(dW/dV)_c b^2} = \pi(S^*), \tag{18}$$

in which S^* is a dimensionless quantity

$$S^* = \frac{S_c}{(dW/dV)_c b} = \frac{r_c}{b}. \tag{19}$$

[4] In general, the quantity δ/b will have to be included:

$$\frac{P}{(dW/dV)_c b^2} = \pi\left[\frac{\delta}{b}, S^*\right].$$

Hence, all geometrically similar structures can be regarded to be governed by S^*. This dimensionless quantity can be used to predict the load versus deflection behavior of all specimen sizes. The amount of subcritical crack growth is obviously size dependent in addition to other influences such as loading steps and material properties. Data on small specimens can thus be collated with those of

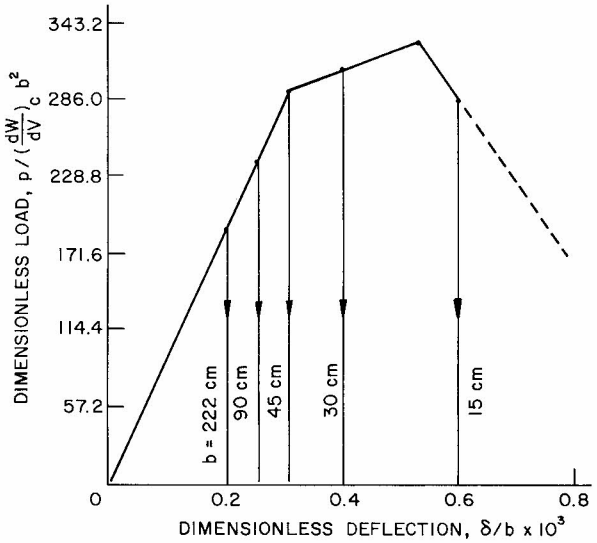

Fig. 16. Dimensionless load-deflection diagram for $\Delta\delta/b = 2.6 \times 10^{-4}$.

larger specimens. There is no need to extrapolate fracture data from the small specimens to the larger ones [13].

5. Additional remarks and conclusions

The foregoing treatment can be regarded as a generalization of the results obtained previously on the basis of the critical stress intensity factor concept [4]. In that work, the transition between structure collapse and failure by brittle fracture was assumed to be governed by the parameter

$$s = \frac{K_{1c}}{\sigma_u \sqrt{b}}, \tag{20}$$

which can be related to S^* in equation (19) as

$$S^* = s^2 \frac{(1+\nu)(1-2\nu)}{\pi}, \tag{21}$$

without considering slow crack growth accompanied by material damage. Therefore, the ideal relation $(dW/dV)_c = \sigma_u^2/2E$ can be used and assumption that local and global instability occur simultaneously. This, of course, cannot always be met in reality.

It is also of interest to discuss the present findings in relation to the maximum load $P_{max}^{(2)}$ results of ASTM [14] for the different b values as

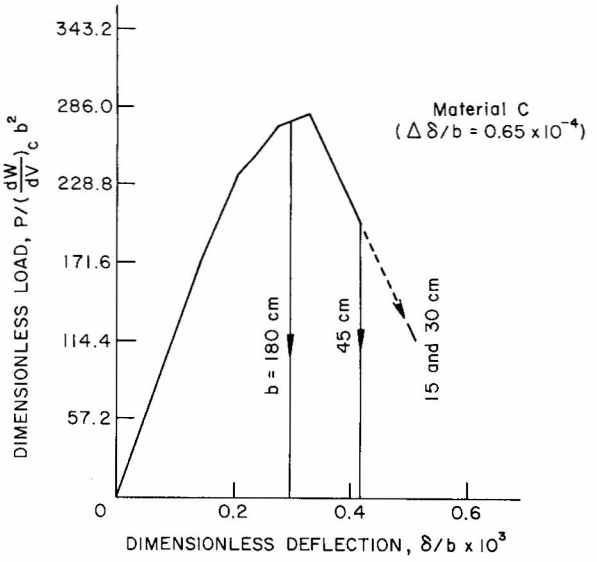

Fig. 18. Dimensionless load-deflection diagram for $\Delta\delta/b = 0.65\times10^{-4}$.

given by the formula

$$K_1 = \frac{Pl}{tb^{3/2}} f(a_0/b), \tag{22}$$

where

$$f\left(\frac{a_0}{b}\right) = 2.9\left(\frac{a_0}{b}\right)^{1/2} - 4.6\left(\frac{a_0}{b}\right)^{3/2} + 21.8\left(\frac{a_0}{b}\right)^{5/2} - 37.6\left(\frac{a_0}{b}\right)^{7/2} + 38.7\left(\frac{a_0}{b}\right)^{9/2}. \tag{23}$$

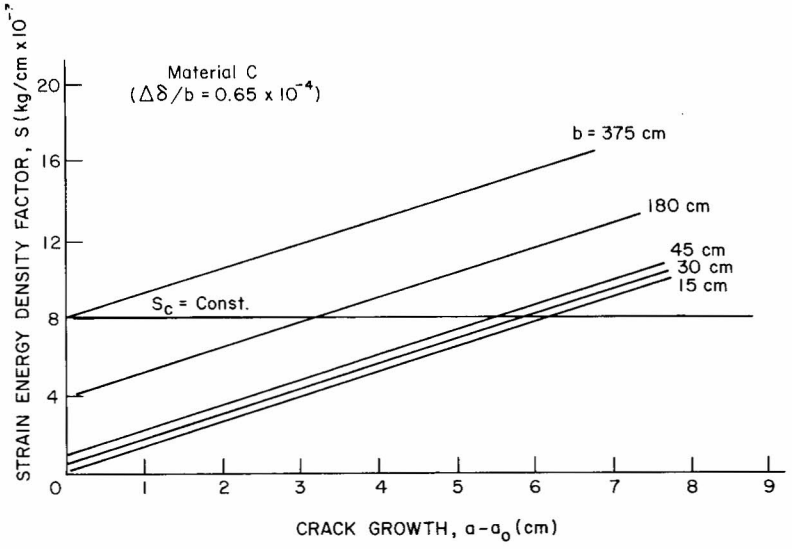

Fig. 17. Strain energy density factor versus crack length for Material C with $\Delta\delta/b = 0.65\times10^{-4}$.

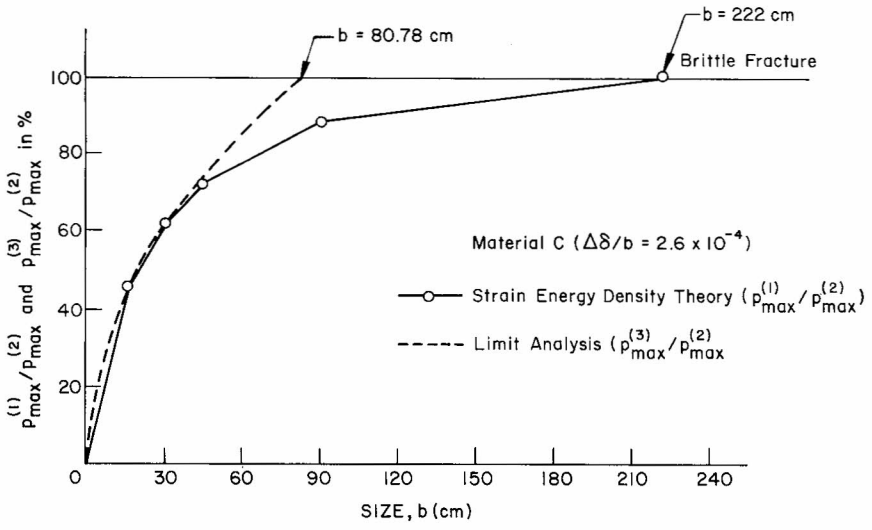

Fig. 19. Comparison of normalized maximum load ratio for brittle fracture and results predicted.

The predicted values of $P^{(3)}_{max}$ from a perfectly-elastic limit analysis are also computed according to

$$P^{(3)}_{max} = \tfrac{2}{3}\frac{\sigma_u t(b-a_0)^2}{l}, \tag{24}$$

where the ligament size at collapse is assumed to be $b - a_0$. Normalizing the results obtained by the present approach $P^{(1)}_{max}$ and $P^{(3)}_{max}$ from equation (24) with that of $P^{(2)}_{max}$ recommended by ASTM and plotting the results against b, Fig. 19 gives a comparison of the predictions in [4] with those obtained in this work. The line $P^{(1)}_{max}/P^{(2)}_{max}$ and $P^{(3)}_{max}/P^{(2)}_{max}$ equal to 100% represents the limiting case of ASTM where failure coincides totally with brittle fracture. The curves in Fig. 19 give the maximum failure load involving both structure collapse and brittle fracture. The model in [4] predicts a transition b value of 80.78 cm while the present model yields $b = 222$ cm. The agreement for the two models is good for $b \leq 45$ cm. This implies that when the specimen size is small, the simple formula in equation (24) gives good prediction based on ultimate strength alone.

In conclusion, it is worthwhile to reiterate that the pseudo-elastic material damage and crack growth model predicts the experimentally observed behavior of concrete-like specimens well. The interactions of loading steps, specimen sizes and different elastic, hardening and softening properties of the material are clearly exhibited from the finite element results for a three-point bend specimen configuration. An important finding is that the condition $dS/da = \text{const.}$ is seen to prevail even though the process of material damage and crack growth is non-self-similar. The idea of dimensional analysis is shown to be useful for resolving the commonly referred to specimen size effect. It suffices to specify the two parameters $(dW/dV)_c$ and S_c whereby the failure behavior of structure collapse and/or brittle fracture can be predicted from the strain energy density theory. The assumption of material homogeneity, of course, has been invoked in this work when applying the present results to concrete structures. There is no fundamental difficulty involved in extending the theory to nonhomogeneous materials [15] except that the finite element stress analysis must be modified to account for changes in the material properties from one grid location to another. Such an effect will be left for future investigations.

References

[1] G.C. Sih, "Mechanics of crack growth: geometrical size effect in fracture", *Fracture Mechanics in Engineering Application*, edited by G.C. Sih and S.R. Valluri, Sijthoff and Noordhoff, pp. 3–29 (1979).

[2] G.C. Sih, "Analytical aspects of macro-fracture mechanics", *Analytical and Experimental Fracture Mechanics*, edited by G.C. Sih and M. Mirabile, Sijthoff and Noordhoff, pp. 3–15 (1981).

[3] A. Carpinteri, "Size effect in fracture toughness testing: a dimensional analysis approach", *Analytical and Experi-*

mental Fracture Mechanics, edited by G.C. Sih and M. Mirabile, Sijthoff and Noordhoff, pp. 785–797 (1981).

[4] A. Carpinteri, "Notch sensitivity in fracture testing of aggregative materials", *Engineering Fracture Mechanics, 16,* pp. 467–481 (1982).

[5] G.C. Sih, "Some basic problems in fracture mechanics and new concepts", *Engineering Fracture Mechanics, 5,* pp. 365–377 (1973).

[6] G.C. Sih and B. Macdonald, "Fracture mechanics applied to engineering problems—strain energy density fracture criterion", *Engineering Fracture Mechanics, 6,* pp. 361–386 (1974).

[7] G.C. Sih and P. Matic, "Mechanical response of materials with physical defects, part 1: modeling of material damage for center cracked panel", *Institute of Fracture and Solid Mechanics Technical Report AFOSR-TR-81-1,* (1981).

[8] G.C. Sih and P. Matic, "Mechanical response of materials with physical defects, part 2: combined modeling of material damage and crack propagation for center cracked panel", *Institute of Fracture and Solid Mechanics Technical Report AFOSR-TR-82-2,* (1982).

[9] G.C. Sih and E. Madenci, "Crack growth resistance characterized by the strain energy density function", *Engineering Fracture Mechanics,* Vol. 18, No. 6, pp. 1159–1171 (1983).

[10] P.D. Hilton, L.N. Gifford and O. Lomacky, "Finite element fracture mechanics of two dimensional and axisymmetric elastic and elastic-plastic cracked structures", *Naval Ship Research and Development Center Report No. 4493,* (1975).

[11] S. Mindess and J.S. Nadeau, "Effect of loading rate on the flexural strength of cement and mortar", *American Ceramic Society Bulletin, 56,* pp. 429–430 (1977).

[12] A. Carpinteri, "Static and energetic fracture parameters for rocks and concretes", *Materials and Structures, 14,* pp. 151–162 (1981).

[13] A. Carpinteri, "Application of fracture mechanics to concrete structures", *Journal of the Structural Division, American Society of Civil Engineers, 108,* pp. 833–848 (1982).

[14] *Standard Method of Test for Plane Strain Fracture Toughness of Metallic Materials,* E 399-74, ASTM.

[15] G.C. Sih, "Mechanics of material damage in concrete", *Fracture Mechanics of Concrete: Material Evaluation and Testing,* edited by A. Carpinteri and A.R. Ingraffea, Martinus Nijhoff Publishers (in press).